PCCP

ROYAL SOCIETY OF CHEMISTRY

PAPER

View Article Online
View Journal | View Issue

Cite this: *Phys. Chem. Chem. Phys.*, 2024, **26**, 21568

Raman optical activity study of deuterated sugars: deuterium labelling as a tool for structural analysis†

Tohru Taniguchi, *[a] Davidson Obinna Agbo,[a] Qin Yang,[b] Josef Kapitán,[c] Tao Wu,[b] Shuki Oyama,[d] Shuji Akai,[d] Yoshinari Sawama[d] and Petr Bouř *[b]

Received 15th June 2024,
Accepted 25th July 2024

DOI: 10.1039/d4cp02406k

rsc.li/pccp

Structural analyses using Raman optical activity (ROA) spectroscopy conventionally rely on vibrational signals in the fingerprint region ranging from 100 to 1800 cm^{-1}. Use of deuterium labelling to observe ROA signals in the C–D stretching region provides additional information about a local structure of large molecular systems. So far, the potential of C–D stretching ROA signals for structural analysis has rarely been explored. In the present work, we synthesized model deuterated glucose monosaccharides and studied their ROA properties by employing molecular dynamics and density functional theory to interpret the spectra. A good agreement between the simulated and experimental spectra is achieved when the proper conformer ratios are considered. This shows the usefulness of ROA spectroscopy assisted by deuterium labelling for stereochemical and conformational analysis.

Introduction

Raman optical activity (ROA) and vibrational circular dichroism (VCD) spectroscopies measure small differences in interactions of a chiral analyte undergoing vibrational transitions with left- *versus* right-circularly polarized light.[1] Each chiral molecule exhibits characteristic ROA and VCD spectral patterns depending on its three-dimensional structures. These techniques, supported by development of theoretical spectral calculations, have allowed one to effectively analyze the structures of various molecular systems. Application of these spectroscopies to small molecules has been successful in obtaining their fine structural property information, such as about stereochemistry of each stereogenic center, conformational ensembles, and solute–solvent interactions.[2] On the other hand, ROA and VCD analysis of larger biomolecules has revealed their secondary and higher-order structures.[3] Both the higher-order and local structure data are of interest for medicinal chemistry, biochemistry, natural product chemistry, *etc.* Nevertheless, the full capability of these spectroscopies for studying local structures (*e.g.*, stereochemistry of a specific stereogenic center in a large molecule, conformation of a ligand bound to its target molecule, and so on) is yet to be explored.

A major obstacle associated with local structural analysis is the signal overlap seen especially in large molecular systems. Most of informative vibrational signals of common molecules are within the fingerprint region approximately ranging from 100 to 1800 cm^{-1}. A narrower range is measured by the current VCD spectrometers (800–1800 cm^{-1}). Small molecules often present sufficiently separated spectral bands in the fingerprint region, enabling one to reliably characterize their fine structures by comparison with calculated spectra. For larger molecules, many different vibrational transitions result in overlapping bands, which makes spectral interpretation difficult. Limitation for distinguishing diastereomers of molecules with multiple stereogenic centers has been pointed out.[4]

Despite these difficulties, determination of local structure is possible when its ROA or VCD signals are selectively detected. For example, structures of photoresponsive chromophores within proteins have been studied by selective observation of chromophoric ROA signals using near-infrared light.[5] Amplification of VCD signals by coordination of a paramagnetic metal ion to an analyte was proposed as a probe of local biomolecular structures.[6] The orientation of N_3^- and CN^- coordinated to the heme iron within proteins has also been studied by observing their stretching VCD signals in the 1900–2400 cm^{-1} region.[7] The use of the 1900–2400 cm^{-1} region, where common molecules do not show the fundamental vibrational transitions, is

[a] *Frontier Research Center for Advanced Material and Life Science, Faculty of Advanced Life Science, Hokkaido University, North 21 West 11, Sapporo 001-0021, Japan. E-mail: ttaniguchi@sci.hokudai.ac.jp*
[b] *Institute of Organic Chemistry and Biochemistry, Academy of Sciences, Flemingovo náměstí 2, 16610 Prague, Czech Republic*
[c] *Department of Optics, Palacký University Olomouc, 17. listopadu 12, 77146 Olomouc, Czech Republic*
[d] *Graduate School of Pharmaceutical Sciences, Osaka University, Suita, Osaka 565-0871, Japan*

† Electronic supplementary information (ESI) available. See DOI: https://doi.org/10.1039/d4cp02406k

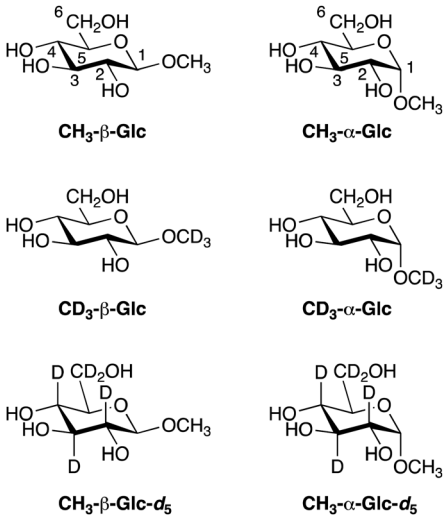

Fig. 1 Structures of glucose derivatives studied in this work.

thus a promising approach to extract information of local structures. Aiming at expanding the capability of these spectroscopies, some of us have been investigating VCD signals of carbon–deuterium (C–D), alkyne, nitrile, isonitrile, allene, carbodiimide, and azido groups within 1900–2400 cm^{-1}.[8] These studies include a study on sugars with the methoxy-d_3 ($-OCD_3$) group such as methyl-d_3-β-D-glucopyranoside (**CD_3-β-Glc**) and methyl-d_3-α-D-glucopyranoside (**CD_3-α-Glc**) (Fig. 1). We found that the configuration at a stereogenic center near the $-OCD_3$ group can be elucidated by solely using the VCD pattern in the C–D stretching region.[8c] Deuterium labelling is an advantageous approach to extract structural information compared to introduction of other chromophores because of its negligible influence on the conformation of the analyte, as exemplified by NMR analysis of deuterated biomolecules.[9] Raman imaging has also been operated to observe C–D stretching signals to monitor the behaviors of labelled molecules in biological systems.[10] These successes motivated us to explore the potential of structural analysis using deuterium labelling by ROA spectroscopy.

Although ROA spectra of deuterated molecules have been reported,[11] the potential of C–D stretching ROA signals as a tool for structural analysis has rarely been studied. This is in part due to difficulties in recording ROA signals in the 1900–2400 cm^{-1} region as common ROA spectrometers are optimized for the fingerprint region. In the present study, with the use of a custom-built ROA spectrometer by one of the authors,[11d,11e,12] we discuss the ROA features of deuterated glucose monosaccharides both in the fingerprint and C–D stretching regions. In particular, this work demonstrates the utility of C–D stretching ROA signals for stereochemical and conformational analyses.

Experimental and computational details

Experimental details

CD_3-β-Glc and **CD_3-α-Glc** were purchased from Aldrich and used without purification. **CD_3-β-Glc**, **CD_3-α-Glc**, **CH_3-β-Glc-d_5**, and **CH_3-α-Glc-d_5** were prepared according to a reported procedure.[8c,13] All sugars were dissolved in water at a concentration of *ca.* 1 M. The backscattered Raman and scattered circular polarization ROA spectra of **CD_3-β-Glc** were acquired with a BioTools ChiralRAMAN-2X instrument at a laser power of 1200 mW for 7 hour. Those of the other molecules were measured on an ROA instrument custom built at the Palacký University, Olomouc,[12a] at a laser power of 260 mW with a measurement time of 4 to 16 hours. Each sample was put in a fused silica cell at an ambient temperature and irradiated by 532 nm excitation laser light.

Computational details on QM/MM-MD calculations

All harmonic DFT calculations were performed using Gaussian 16,[14] while MD simulations were run on the AMBER18 program.[15] Initial structures were optimized at the B3LYP/6-31G(d) level, and then submitted for MD simulations with incorporating *ca.* 170 water molecules employing periodic boundary conditions and an octahedral cell. The GLYCAM force field was selected, and water molecules were modelled using the TIP3P potential.

In a preparatory MD step, two stages of system optimization were performed. In the first stage, energy minimization of the octahedral model was conducted with 500 steps of the steepest descent followed by 500 steps of the conjugate gradient method. The smooth particle-mesh Ewald method was used for electrostatic interactions, van der Waals and electrostatic interactions were set with a cutoff distance of 6 Å, and a restraining force of 500 kcal mol^{-1} was applied to the atoms of sugar molecules. In the second stage, 1000 steps of the steepest descent were followed by 2500 steps of the conjugate gradient method to optimize the sugars without constraints.

Subsequently, NVT and NPT equilibration and MD simulations were performed. Initially, 20 ps of equilibration at constant volume was carried out, applying a weak constraining force of 10 kcal mol^{-1} to the sugar molecules. The temperature was raised from 0 K to 300 K using the Langevin thermostat and maintained at 300 K thereafter. The SHAKE algorithm was applied to constrain bonds involving hydrogen atoms, with a time step of 2 fs. Production simulation involved a 9 ns run under similar conditions, with some modifications: all constraints were removed from the sugar molecules, the temperature was maintained at 300 K using the Langevin method, and the pressure was kept at 1 atm. Upon completion of the simulation, 50 snapshots were taken for each system, with one snapshot every 50 ps within the 2500–4500 ps interval.

Next, geometry optimizations of the 50 snapshots were performed. A two-layer ONIOM method was utilized for the QM/MM calculations. The solute was calculated at the B3LYP/spAug-cc-pVDZ level, while the water molecules were represented by the AMBER force field. Following the optimization, vibrational frequencies and Raman and ROA intensities were calculated at the same level as used for optimization. The calculated intensities were plotted as Raman and ROA spectra using a half-width at half-height of 10 cm^{-1}. Final spectra were obtained by averaging the spectra of these 50 geometries.

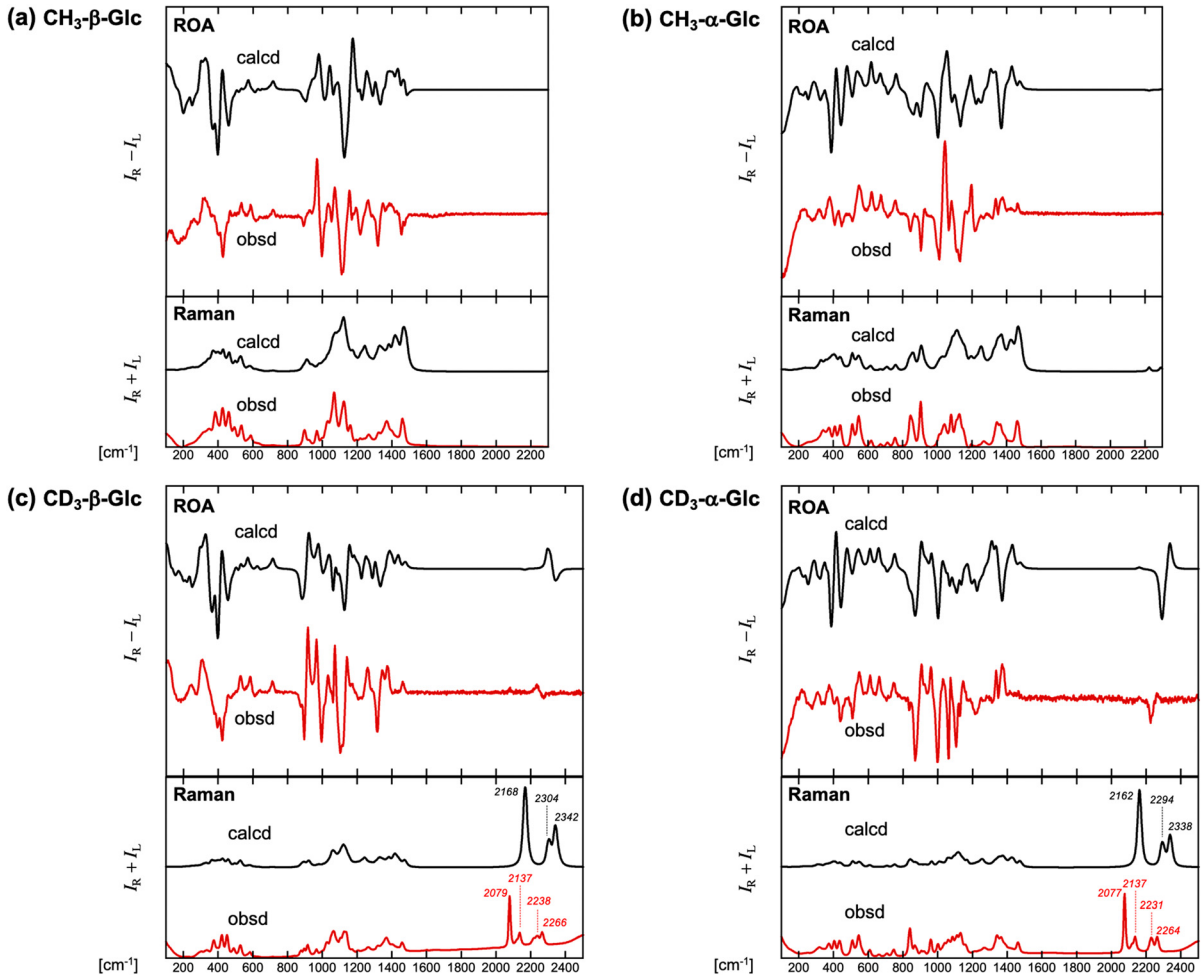

Fig. 2 Observed (red) and calculated QM/MM (harmonic approximation, black) ROA and Raman spectra of (a) **CH_3-β-Glc**, (b) **CH_3-α-Glc**, (c) **CD_3-β-Glc**, and (d) **CD_3-α-Glc**. Wavenumbers for Raman peak tops in the C–D stretching region are indicated.

Computational details on PCM calculations

Molecular mechanics conformational search was performed for each molecule using Spartan'20 software.[16] Geometries within 20 kJ mol^{-1} from the most stable conformation were then submitted for DFT optimization and spectral calculations at the B3LYP/spAug-cc-pVDZ level with the polarizable continuum model (PCM) for water. For each molecule, three most stable conformers were considered for the spectral calculations. The ROA spectra of each conformer were averaged according to the Boltzmann populations simulated at 298 K.

Generalized second-order vibrational perturbation theory (GVPT2)[17] as implemented in Gaussian was used for considering the anharmonic effects. The anharmonic force field and polarizability derivatives were calculated at the B3LYP/spAug-cc-pVDZ level, with the normal mode differentiation step of $0.01\sqrt{\text{amu}}\cdot\text{bohr}$. PCM with United Atom Topological Model (UA0 PCM) was used to simulate the solvent effects.[18] Resonance analysis was done using a modified version of Gaussian,[19] with the energy criteria for Fermi and Darling Dennison resonances of 200 cm^{-1} and 100 cm^{-1}, respectively; the intensity criteria were $K^{1-2} = 1/K_I^{1-2} = 0.1$ and $K^{1-1} = 1/K_I^{1-1} = 0.3$, respectively.[20]

Results and discussion

Deuterated and unlabelled glucose monosaccharides studied in this work are shown in Fig. 1. The ROA spectrum of methyl-β-D-glucopyranoside (**CH_3-β-Glc**) was previously reported both for the fingerprint region as well as for the C–H stretching region.[21] QM/MM calculations of the ROA spectrum of **CH_3-β-Glc** surrounded by many explicit water molecules were also reported.[21b,21c] Experimental ROA spectrum of methyl-α-D-glucopyranoside (**CH_3-α-Glc**) was reported only in the 600–1400 cm^{-1} region without theoretical calculations.[21a]

The synthesis of **CD_3-β-Glc** and **CD_3-α-Glc** was performed using a reported procedure.[8c] Methyl-β-D-glucopyranoside-d_5 (**CH_3-β-Glc-d_5**) and methyl-α-D-glucopyranoside-d_5 (**CH_3-α-Glc-d_5**) were prepared using a selective Ru/C-catalyzed H–D exchange reaction.[13]

Experimental spectra of unlabelled and d_3-methylated glucoses

Fig. 2 shows the ROA and Raman spectra of H_2O solutions of **CH_3-β-Glc**, **CH_3-α-Glc**, **CD_3-β-Glc**, and **CD_3-α-Glc**. Their ROA and Raman intensities are expressed in arbitrary units. The

experimental Raman and ROA spectra of **CH_3-β-Glc** and **CH_3-α-Glc** are similar to previously reported ones (Fig. 2a and b).[21] The Raman spectra of the isotopologues **CD_3-β-Glc** and **CD_3-α-Glc** are somewhat similar to those of **CH_3-β-Glc** and **CH_3-α-Glc**, respectively, in the fingerprint region, with major differences seen in the 800–1200 cm^{-1} region (Fig. 2c and d). In the C–D stretching region, both **CD_3-β-Glc** and **CD_3-α-Glc** exhibit intense Raman peaks: 2079, 2137, 2238, and 2266 cm^{-1} for **CD_3-β-Glc** and 2077, 2137, 2231, and 2264 cm^{-1} for **CD_3-α-Glc**. The transitions at 2079 and 2238 cm^{-1} for **CD_3-β-Glc** and at 2077 and 2231 cm^{-1} for **CD_3-α-Glc** are known to be associated with VCD signals with moderate intensity, whose sign patterns were reversed depending on the stereochemistry at C-1.[8c] The ROA signal at 2079/2077 cm^{-1} is negligibly small. The modes at 2238/2231 cm^{-1} and 2266/2264 cm^{-1} form a bisignate ROA pattern. **CD_3-β-Glc** shows a positive peak at 2238 cm^{-1} and a negative one at 2266 cm^{-1}, whereas **CD_3-α-Glc** presents a negative one at 2231 cm^{-1} and a positive one at 2264 cm^{-1}. Thus, the ROA patterns of these two molecules in the C–D stretching region are almost opposite, even though these are diastereomers differing only in the stereochemistry at C-1. This result suggests that their C–D stretching ROA pattern serves as a promising probe of local structures.

Theoretical spectra of unlabelled and d_3-methylated glucoses

In an ideal scenario, local structure of a target molecule would be determined directly by interpreting the spectrum. Therefore, we examined whether the C-1 stereochemistry of the deuterated sugars can be elucidated by comparison of experimental and theoretical ROA spectra in the C–D stretching region. Theoretical calculations of Raman and ROA spectra were carried out for **CD_3-β-Glc** and **CD_3-α-Glc** as well as for **CH_3-β-Glc** and **CH_3-α-Glc**. Unlabelled sugars were studied to better understand their ROA properties in the fingerprint region in comparison to labelled ones.

Analysis of MD results shows that the conformer ratios regarding the C-6 hydroxymethyl group (gg : gt : tg) are 58 : 42 : 0 for **CH_3-β-Glc** and 46 : 54 : 0 for **CH_3-α-Glc**. There ratios are close to experimentally estimated values.[22] The following QM calculations were performed using the DFT/B3LYP/spAug-cc-pVDZ level because, amongst the tested conditions, it produced the best spectra upon comparison with the experimental one (Fig. S1, ESI†). We used 50 MD snapshots to obtain the final spectra as consideration of 100 snapshots did not seem to improve the agreement with the observed ones (Fig. S2a, ESI†). In Fig. 2, the Raman and ROA intensities of the theoretical spectra are arbitrarily scaled, whereas the frequencies are unscaled.

Previous QM/MM calculations of **CH_3-β-Glc** well reproduced its experimental ROA spectral pattern.[21b,21c] In this work as well, the calculated and observed ROA spectra of **CH_3-β-Glc** in Fig. 2a show almost one-to-one band correspondence. Disagreement is seen for the predicted positive ROA band at 424 cm^{-1} and negative one at 456 cm^{-1}, mostly ascribed to C–O–H twisting modes. These bisignate signals may be cancelled out in the observed spectrum.

Table 1 Frequencies of the pair of positive and negative ROA signals originating from antisymmetric OCD_3 stretching of **CD_3-β-Glc** and **CD_3-α-Glc**

	CD_3-β-Glc		**CD_3-α-Glc**	
	Positive [cm^{-1}]	Negative [cm^{-1}]	Negative [cm^{-1}]	Positive [cm^{-1}]
Observed	2235	2275	2230	2260
Harmonic (QM/MM)	2298	2344	2292	2336
Harmonic (PCM)	2320	2358	2302	2342
Anharmonic (PCM)	2206	2248	2203	2246

To our knowledge, calculations of the ROA spectrum of **CH_3-α-Glc** have not been conducted. We have performed them using the QM/MM and by PCM approaches. With QM/MM, although discrepancies are seen for ROA spectra in the regions around 400 cm^{-1} and 1400 cm^{-1}, reasonable overall agreement between the theoretical and experimental spectra is achieved (Fig. 2b). Assignment of the vibrational bands is summarized in Table S1 (ESI†). The QM/MM method led a better qualitative and quantitative agreement compared to PCM (Fig. S2b, ESI†).

Having confirmed reasonable agreement in the fingerprint region of **CH_3-β-Glc** and **CH_3-α-Glc**, we then examined the spectra of isotopologues **CD_3-β-Glc** and **CD_3-α-Glc**. In the fingerprint region, the calculated and measured ROA spectra of **CD_3-β-Glc** showed a good agreement, with differences associated with the C–O–H twisting modes seen around 400 cm^{-1} (Fig. 2c). As for **CD_3-α-Glc**, the agreement between the theoretical and experimental ROA spectra is moderate; especially, the 400 cm^{-1} and 1400 cm^{-1} regions showed noticeable discrepancies (Fig. 2d), in a similar manner to the case of **CH_3-α-Glc**. In the C–D stretching region, the calculated ROA spectra of both **CD_3-β-Glc** and **CD_3-α-Glc** presented patterns similar to the observed ones. **CD_3-β-Glc** shows a pair of positive and then negative signals from lower to higher frequency, whereas **CD_3-α-Glc** exhibits a negative to positive pattern (see Fig. S3 for the corresponding vibrational modes, ESI†). These results suggest that the local structure (in this case C-1 stereochemistry) of deuterated sugars can be determined by the comparison of theoretical and experimental ROA signals originating from the C–D stretching vibrations.

Although the vibrations within the 1900–2400 cm^{-1} region are prone to anharmonic effects such as overtone and combination bands,[8d,12b,23] in our case harmonic calculations were found satisfactory for prediction of the spectral shapes for **CD_3-β-Glc** and **CD_3-α-Glc**. Most probably, many anharmonic effects were averaged out because of molecular flexibility and the strongly interacting polar environment, as observed also for similar systems.[21c] However, calculated harmonic frequencies of the C–D stretching modes were much higher than the experimental ones (Table 1). Moreover, experimental Raman spectra of both **CD_3-β-Glc** and **CD_3-α-Glc** showed an additional signal at 2137 cm^{-1} that was not reproduced by the harmonic approach.

To see whether experimental ROA and Raman spectra in the C–D stretching region can be better reproduced, we performed anharmonic GVPT2 calculations.[12b,17a,20] Anharmonic theoretical

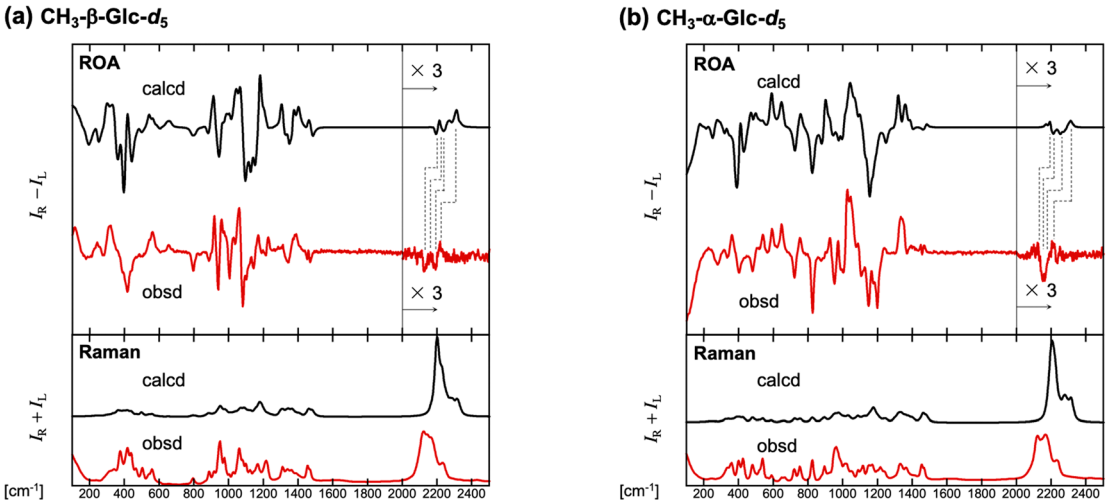

Fig. 3 Observed (red) and harmonically calculated (black) ROA and Raman spectra of (a) **CH_3-β-Glc-d_5** and (b) **CH_3-α-Glc-d_5**. The intensity of ROA spectra above 2000 cm^{-1} is multiplied by a factor of 3 for clarity.

ROA spectra showed a pair of positive and negative signals in the C–D stretching region in the same sign order of the observed (Fig. S4, ESI†). As listed in Table 1, predicted frequencies by GVPT2 were closer to the experimental values compared to the harmonic predictions. Anharmonic calculations of Raman spectra also reproduced some of the observed features. However, the overall agreement between their anharmonic theoretical Raman and ROA spectra and experimental ones remains to be improved in future studies (see the caption of Fig. S4, ESI†).

Experimental and theoretical spectra of d_5-glucoses

Our results on **CD_3-β-Glc** and **CD_3-α-Glc** showed the feasibility of ROA spectroscopy to analyze the local structure in the vicinity of a deuterated site. However, ROA intensity originating from the $-OCD_3$ group is relatively weak, which may hamper analysis of deuterated molecules with poor solubility or available in small amounts. Because of the limited number of ROA studies in the 1900–2400 cm^{-1} region, molecular system yielding strong C–D stretching ROA signals is not known. In the field of Raman imaging, weak Raman intensity of the C–D stretching modes has been compensated by introduction of multiple deuterium atoms (*e.g.*, d_{29}-γ-linoleic acid and d_8-methionine).[10] To see the behavior of ROA signals of molecules with a larger number of deuterium atoms, we next studied **CH_3-β-Glc-d_5** and **CH_3-α-Glc-d_5**.

Fig. 3 shows the Raman and ROA spectra of **CH_3-β-Glc-d_5** and **CH_3-α-Glc-d_5**. Both molecules show significantly different Raman and ROA spectral patterns compared to their unlabelled counterparts **CH_3-β-Glc** and **CH_3-α-Glc** even in the fingerprint region, especially within 400–1600 cm^{-1}. This is consistent with previous[21b] and our vibrational assignments, which suggests that many of the vibrational modes in this region are associated with C–H motions (Table S1, ESI†). In the C–D stretching region, both **CH_3-β-Glc-d_5** and **CH_3-α-Glc-d_5** exhibit strong, relatively broad Raman bands, whereas their ROA intensity remains mediocre despite the introduction of five deuterium atoms. Their intensity is not particularly smaller than some of the signals in the fingerprint region, but these are more difficult to measure. This is because the ROA/Raman ratio is small, as the ROA noise is approximately proportional to the Raman signal.

To examine the possibility of interpretation of these ROA patterns, QM/MM spectral calculations were performed. Theoretical ROA spectra of **CH_3-β-Glc-d_5** and **CH_3-α-Glc-d_5** by harmonic QM/MM-MD method are in a good agreement with the observed ones in the fingerprint region, although some differences are seen again in the region around 400 cm^{-1}. In the C–D stretching region, the observed ROA patterns are also moderately reproduced by the calculations. Analysis of the QM/MM-MD spectra of selected snapshots found that their C–D stretching ROA patterns are dependent on the conformation (Fig. S5, ESI†). For example, *gg* conformers of **CH_3-α-Glc-d_5** yield a positive ROA signal at around 2200 cm^{-1}, whereas its *gt* conformers tend to produce a negative one (see Fig. S5c for the calculated ROA spectra of selected snapshots, ESI†). This result suggests that the cancellation of signals of opposite signs for the conformers contributes to the weak intensity of the C–D stretching ROA signals of **CH_3-β-Glc-d_5** and **CH_3-α-Glc-d_5** seen in Fig. 3. Despite the relatively weak intensity, the results confirm the sensitivity of the C–D stretching ROA signals to conformation, which will be useful for conformational analyses.

Conclusions

Through ROA studies on deuterated glucose monosaccharides, we could, in detail, investigate the ROA spectra of C–D stretching modes and their relation to the structure. ROA spectra in the C–D stretching region of **CD_3-β-Glc** and **CD_3-α-Glc** were almost mirror-image to each other, which confirms their usefulness and sensitivity to the configuration at the closest stereogenic center. Similarly, on the differently deuterated **CH_3-β-Glc-d_5** and **CH_3-α-Glc-d_5**, we demonstrate the sensitivity

of the C–D stretching signals to conformation. The harmonic approximation produced spectra satisfactory for the interpretation of the experimental C–D stretching ROA signals for all tested molecules. The perturbative anharmonic calculations indicate that inclusion of the anharmonic effects may improve the theoretical frequencies. Overall, this work provides a deep insight into the link between the structure and ROA signals of the C–D stretching vibrations. This can be useful for future studies on local structural analysis of deuterated moiety in larger molecular systems with or without combining other methods such as selective excitation[5] and signal augmentation.[24]

Data availability

The data supporting this article have been included as part of the ESI.†

Conflicts of interest

There are no conflicts to declare.

Acknowledgements

This work was supported by KAKENHI (Grant No. 18H02093, 18KK0394, and 23H02089) and by Czech grant agency (Grant No. 24-10558S). D. O. A. is grateful for a scholarship from the Ministry of Education, Culture, Sports, Science and Technology, Japan. QY thanks the financial support from fellowship from Institute of Organic Chemistry and Biochemistry, Czech Academy of Science, and the COST Action CA21101 "*COSY–Confined molecular systems: from a new generation of materials to the stars*". Prof. Kenji Monde is acknowledged for discussion of experimental ROA spectra. Prof. Julien Bloino is also acknowledged on the discussion and local modified version of Gaussian on anharmonic simulation.

Notes and references

1 (*a*) L. A. Nafie, *Vibrational optical activity: principles and applications*, Wiley, Chichester England; Syracuse, N. Y, 2011; (*b*) M. Krupová, J. Kessler and P. Bouř, *ChemPlusChem*, 2020, **85**, 561–575.

2 (*a*) Y. He, B. Wang, R. K. Dukor and L. A. Nafie, *Appl. Spectrosc.*, 2011, **65**, 699–723; (*b*) J. M. Batista, E. W. Blanch and V. D. Bolzani, *Nat. Prod. Rep.*, 2015, **32**, 1280–1302; (*c*) A. S. Perera, J. Thomas, M. R. Poopari and Y. Xu, *Front. Chem.*, 2016, **4**, 9; (*d*) C. Merten, *Phys. Chem. Chem. Phys.*, 2017, **19**, 18803–18812; (*e*) P. L. Polavarapu and E. Santoro, *Nat. Prod. Rep.*, 2020, **37**, 1661–1699.

3 (*a*) L. D. Barron and L. Hecht, *Comprehensive Chiroptical Spectroscopy*, 2012, pp. 759–793, DOI: **10.1002/9781118120392.ch23**; (*b*) A. Rüther, A. Forget, A. Roy, C. Carballo, F. Mießmer, R. K. Dukor, L. A. Nafie, C. Johannessen, V. P. Shastri and S. Lüdeke, *Angew. Chem., Int. Ed.*, 2017, **56**, 4603–4607; (*c*) T. A. Keiderling, *Chem. Rev.*, 2020, **120**, 3381–3419.

4 B. Simmen, T. Weymuth and M. Reiher, *J. Phys. Chem. A*, 2012, **116**, 5410–5419.

5 (*a*) M. Unno, T. Kikukawa, M. Kumauchi and N. Kamo, *J. Phys. Chem. B*, 2013, **117**, 1321–1325; (*b*) T. Fujisawa, R. L. Leverenz, M. Nagamine, C. A. Kerfeld and M. Unno, *J. Am. Chem. Soc.*, 2017, **139**, 10456–10460.

6 S. R. Domingos, A. Huerta-Viga, L. Baij, S. Amirjalayer, D. A. E. Dunnebier, A. J. C. Walters, M. Finger, L. A. Nafie, B. de Bruin, W. J. Buma and S. Woutersen, *J. Am. Chem. Soc.*, 2014, **136**, 3530–3535.

7 (*a*) C. Marcott, H. A. Havel, B. Hedlund, J. Overend and A. Moscowitz, in *Optical Activity and Chiral Discrimination: Proceedings of the NATO Advanced Study Institute held at the University of Sussex, Falmer, England, 1978*, ed. S. F. Mason, Springer Netherlands, Dordrecht, 1979, DOI: **10.1007/978-94-015-7644-4_11**, pp. 289–292; (*b*) J. Teraoka, K. Nakamura, Y. Nakahara, Y. Kyogoku and H. Sugeta, *J. Am. Chem. Soc.*, 1992, **114**, 9211–9213.

8 (*a*) T. Taniguchi, T. Suzuki, H. Satoh, Y. Shichibu, K. Konishi and K. Monde, *J. Am. Chem. Soc.*, 2018, **140**, 15577–15581; (*b*) T. Taniguchi, M. Z. M. Zubir, N. Harada and K. Monde, *Phys. Chem. Chem. Phys.*, 2021, **23**, 27525–27532; (*c*) M. Z. M. Zubir, N. F. Maulida, Y. Abe, Y. Nakamura, M. Abdelrasoul, T. Taniguchi and K. Monde, *Org. Biomol. Chem.*, 2022, **20**, 1067–1072; (*d*) T. Taniguchi and D. O. Agbo, *Phys. Chem. Chem. Phys.*, 2023, **25**, 28567–28575; (*e*) T. Taniguchi, Mutmainah, S. Takimoto, T. Suzuki, S. Watanabe, F. Matsuda, T. Umezawa and K. Monde, *Org. Biomol. Chem.*, 2023, **21**, 569–574.

9 M. Kainosho, T. Torizawa, Y. Iwashita, T. Terauchi, A. Mei Ono and P. Güntert, *Nature*, 2006, **440**, 52–57.

10 (*a*) K. Dodo, A. Sato, Y. Tamura, S. Egoshi, K. Fujiwara, K. Oonuma, S. Nakao, N. Terayama and M. Sodeoka, *Chem. Commun.*, 2021, **57**, 2180–2183; (*b*) S. J. Spratt, T. Mizuguchi, H. Akaboshi, H. Kosakamoto, R. Okada, F. Obata and Y. Ozeki, *Front. Chem.*, 2023, **11**, 1141920.

11 (*a*) J. Haesler, I. Schindelholz, E. Riguet, C. G. Bochet and W. Hug, *Nature*, 2007, **446**, 526–529; (*b*) M. Pazderková, V. Profant, J. Hodačová, J. Šebestík, T. Pazderka, P. Novotná, M. Urbanová, M. Šafařík, M. Buděšínský, M. Tichý, L. Bednárová, V. Baumruk and P. Maloň, *J. Phys. Chem. B*, 2013, **117**, 9626–9642; (*c*) J. Šebestík, F. Teplý, I. Císařová, J. Vávra, D. Koval and P. Bouř, *Chem. Commun.*, 2016, **52**, 6257–6260; (*d*) M. Hope, J. Šebestík, J. Kapitán and P. Bouř, *J. Phys. Chem. A*, 2020, **124**, 674–683; (*e*) T. Brotin, N. Daugey, J. Kapitán, N. Vanthuyne, M. Jean, E. Jeanneau and T. Buffeteau, *J. Org. Chem.*, 2023, **88**, 4829–4832.

12 (*a*) P. Michal, R. Čelechovský, M. Dudka, J. Kapitán, M. Vůjtek, M. Berešová, J. Šebestík, K. Thangavel and P. Bouř, *J. Phys. Chem. B*, 2019, **123**, 2147–2156; (*b*) Q. Yang, J. Kapitán, P. Bouř and J. Bloino, *J. Phys. Chem. Lett.*, 2022, **13**, 8888–8892.

13 Y. Sawama, Y. Yabe, H. Iwata, Y. Fujiwara, Y. Monguchi and H. Sajiki, *Chem. – Eur. J.*, 2012, **18**, 16436–16442.

14 M. J. Frisch, G. W. Trucks, H. B. Schlegel, G. E. Scuseria, M. A. Robb, J. R. Cheeseman, G. Scalmani, V. Barone, G. A. Petersson, H. Nakatsuji, X. Li, M. Caricato, A. V. Marenich, J. Bloino, B. G. Janesko, R. Gomperts, B. Mennucci, H. P. Hratchian, J. V. Ortiz, A. F. Izmaylov, J. L. Sonnenberg, D. Williams-Young, F. Ding, F. Lipparini, F. Egidi, J. Goings, B. Peng, A. Petrone, T. Henderson, D. Ranasinghe, V. G. Zakrzewski, J. Gao, N. Rega, G. Zheng, W. Liang, M. Hada, M. Ehara, K. Toyota, R. Fukuda, J. Hasegawa, M. Ishida, T. Nakajima, Y. Honda, O. Kitao, H. Nakai, T. Vreven, K. Throssell, J. A. Montgomery, Jr., J. E. Peralta, F. Ogliaro, M. J. Bearpark, J. J. Heyd, E. N. Brothers, K. N. Kudin, V. N. Staroverov, T. A. Keith, R. Kobayashi, J. Normand, K. Raghavachari, A. P. Rendell, J. C. Burant, S. S. Iyengar, J. Tomasi, M. Cossi, J. M. Millam, M. Klene, C. Adamo, R. Cammi, J. W. Ochterski, R. L. Martin, K. Morokuma, O. Farkas, J. B. Foresman and D. J. Fox, *Gaussian 16, Revision C.02*, Gaussian, Inc., Wallingford CT, 2019.

15 D. A. Case, I. Y. Ben-Shalom, S. R. Brozell, D. S. Cerutti, T. E. Cheatham, III, V. W. D. Cruzeiro, T. A. Darden, R. E. Duke, D. Ghoreishi, M. K. Gilson, H. Gohlke, A. W. Goetz, D. Greene, R. Harris, N. Homeyer, Y. Huang, S. Izadi, A. Kovalenko, T. Kurtzman, T. S. Lee, S. LeGrand, P. Li, C. Lin, J. Liu, T. Luchko, R. Luo, D. J. Mermelstein, K. M. Merz, Y. Miao, G. Monard, C. Nguyen, H. Nguyen, I. Omelyan, A. Onufriev, F. Pan, R. Qi, D. R. Roe, A. Roitberg, C. Sagui, S. Schott-Verdugo, J. Shen, C. L. Simmerling, J. Smith, R. Salomon- Ferrer, J. Swails, R. C. Walker, J. Wang, H. Wei, R. M. Wolf, X. Wu, L. Xiao, D. M. York and P. A. Kollman, *AMBER 2018*, University of California, San Francisco, 2018.

16 *Spartan'20*, Wavefunction, Inc., Irvine, CA.

17 (*a*) J. Bloino, M. Biczysko and V. Barone, *J. Phys. Chem. A*, 2015, **119**, 11862–11874; (*b*) M. Piccardo, J. Bloino and V. Barone, *Int. J. Quantum Chem.*, 2015, **115**, 948–982.

18 V. Barone, M. Cossi and J. Tomasi, *J. Chem. Phys.*, 1997, **107**, 3210–3221.

19 M. J. Frisch, G. W. Trucks, G. Scalmani, J. R. Cheeseman, X. Li, J. Bloino, B. G. Janesko, A. V. Marenich, J. Zheng, F. Lipparini, A. Jenkins, A. Liu, H. Liu, H. B. Schlegel, G. E. Scuseria, M. A. Robb, V. Barone, G. A. Petersson, H. Nakatsuji, B. Mennucci, C. Adamo, N. Rega, M. Caricato, H. P. Hratchian, J. V. Ortiz, A. F. Izmaylov, H. Hu, C. Liao, J. L. Sonnenberg, D. Williams-Young, F. Ding, R. Gomperts, F. Egidi, J. Goings, B. Peng, A. Petrone, T. Henderson, D. Ranasinghe, V. G. Zakrzewski, J. Gao, G. Zheng, W. Liang, M. Hada, M. Ehara, K. Toyota, R. Fukuda, J. Hasegawa, M. Ishida, T. Nakajima, Y. Honda, O. Kitao, H. Nakai, T. Vreven, K. Throssell, J. A. Montgomery, Jr., J. E. Peralta, F. Ogliaro, M. J. Bearpark, J. J. Heyd, E. N. Brothers, K. N. Kudin, V. N. Staroverov, T. A. Keith, R. Kobayashi, J. Normand, K. Raghavachari, A. P. Rendell, J. C. Burant, S. S. Iyengar, M. Cossi, J. M. Millam, M. Klene, R. Cammi, R. L. Martin, O. Farkas, J. B. Foresman and D. J. Fox, *Gaussian Development Version, Revision J.25*, 2023, Gaussian, Inc., Wallingford CT.

20 Q. Yang and J. Bloino, *J. Phys. Chem. A*, 2022, **126**, 9276–9302.

21 (*a*) Z. Q. Wen, L. D. Barron and L. Hecht, *J. Am. Chem. Soc.*, 1993, **115**, 285–292; (*b*) J. R. Cheeseman, M. S. Shaik, P. L. A. Popelier and E. W. Blanch, *J. Am. Chem. Soc.*, 2011, **133**, 4991–4997; (*c*) V. Palivec, V. Kopecký, P. Jungwirth, P. Bouř, J. Kaminský and H. Martinez-Seara, *Phys. Chem. Chem. Phys.*, 2020, **22**, 1983–1993.

22 (*a*) Y. Nishida, H. Ohrui and H. Meguro, *Tetrahedron Lett.*, 1984, **25**, 1575–1578; (*b*) Y. Nishida, H. Hori, H. Ohrui and H. Meguro, *J. Carbohydr. Chem.*, 1988, **7**, 239–250; (*c*) K. Bock and J. Ø. Duus, *J. Carbohydr. Chem.*, 1994, **13**, 513–543.

23 (*a*) P. L. Polavarapu, L. A. Nafie, S. A. Benner and T. H. Morton, *J. Am. Chem. Soc.*, 1981, **103**, 5349–5354; (*b*) S. Abbate, H. A. Havel, L. Laux, V. Pultz and A. Moscowitz, *J. Phys. Chem.*, 1988, **92**, 3302–3311; (*c*) A. J. Schmitz, D. G. Hogle, X. S. Gai, E. E. Fenlon, S. H. Brewer and M. J. Tucker, *J. Phys. Chem. B*, 2016, **120**, 9387–9394.

24 (*a*) S. Abdali and E. W. Blanch, *Chem. Soc. Rev.*, 2008, **37**, 980–992; (*b*) M. Das, D. Gangopadhyay, J. Šebestík, L. Habartová, P. Michal, J. Kapitán and P. Bouř, *Chem. Commun.*, 2021, **57**, 6388–6391.

